Journal of South American Earth Sciences 29 (2010) 772–783

Contents lists available at ScienceDirect

Journal of South American Earth Sciences

journal homepage: www.elsevier.com/locate/jsames

Permian to Triassic I to S-type magmatic switch in the northeast Sierra Nevada de Santa Marta and adjacent regions, Colombian Caribbean: Tectonic setting and implications within Pangea paleogeography

A. Cardona [a,b,*], V. Valencia [c], A. Garzón [d], C. Montes [a], G. Ojeda [b], J. Ruiz [c], M. Weber [e]

[a] Smithsonian Tropical Research Institute, Ancón, Panama
[b] Instituto Colombiano del Petróleo, Ecopetrol, Piedecuesta, Colombia
[c] Department of Geosciences, University of Arizona, Tucson, USA
[d] Departamento de Geociéncias, Universidad Nacional, Bogotá, Colombia
[e] Escuela de Geociénicas y Medio Ambiente, Universidad Nacional, Medellín, Colombia

ARTICLE INFO

Article history:
Received 25 August 2008
Accepted 28 December 2009

Keywords:
Pangea
Subduction
Accretion
Geochemistry
U–Pb geochronology

ABSTRACT

The Late Paleozoic to Triassic tectonics of northwestern South America have major implications for the understanding of Laurentia–Gondwana interactions that formed Pangea, and the origin of several tectonostratigraphic terranes dispersed by the break-up of this supercontinent during the formation of the Caribbean. Two mylonitic and orthogneissic granitoid suites have been recognized in the northeastern segment of the Sierra Nevada de Santa Marta, the lower Magdalena basin and the Guajira Serranias, within the Caribbean region of Colombia. For the Santa Marta region U/Pb LAM-ICP-MS analysis yielded zircon crystallization ages of 288.1 ± 4.5 Ma, 276.5 ± 5,1 Ma and 264.9 ± 4.0 Ma, related to the magmatic intrusion. Geochemical and modal variations show a compositional spectrum between diorite and granite, whereas LREE enrichment, Ti and Nb anomalies and geochemical discrimination suggest that this granitoid suite was formed within a magmatic arc setting. Inherited zircons suggest that this Early Permian plutonism was formed with the participation of Neoproterozoic and Grenvillian basement proximal to the South American continent. Evidence of a superimposed Early Triassic (ca. 250 Ma) deformational event in Santa Marta, together with a well defined S-type magmatism in the basement rocks from the adjacent lower Magdalena Valley and Guajira Peninsula regions are related to a major shift in the regional tectonic evolution. It's envisioned that this event records either terrane accretion or strong plate coupling during the final stages of Pangea agglutination. Connections with the main Alleghanian-Ouachitan Pangean orogen are precluded due to their timing differences. The plutons temporally and compositionally correlate with an arc found in the northern Andes and Mexican Gondwana terranes, and represent a broader magmatic event formed at the proto-Pacific margin, outside the nucleus of the Laurentia–Gondwana Alleghanian-Oachitan orogens. Evidence of lower temperature recrystallization is probably linked to a younger Late Cretaceous deformational event that reworked the margin during the accretion of the Caribbean arc to the northwest of South America.

1. Introduction

Late Paleozoic to Triassic tectonics of the proto-Andean margin are related to the final stages of agglutination of the Pangea supercontinent and the evolution of an active subduction zone along its outboard Pacific margin (reviews in Hatcher (2002), Poole et al. (2005), Cawood and Buchan (2007)). Regional paleogeographic reconstructions for Pangea up until the Jurassic have suggested that the northern South American margin was in geographic proximity with Laurentia, with several southern Mexico and Middle Americas terranes probably linked to the northern Andean margin and its associated terranes (Pindell and Dewey, 1982; Pindell, 1985; Rowley and Pindell, 1989; Toussaint, 1993; Ruiz et al., 1999; Stewart et al., 1999; Dickinson and Lawton, 2001; Torsvik and Cocks, 2004). Recent geological and geochronological data from magmatic and migmatitic rocks of the Northern Andes have shown that the Late Paleozoic to Triassic tectonic event was extensively recorded from northern Peru to the Central Cordillera of the Colombian Andes (Restrepo et al., 1991; Noble et al., 1997; Torres et al., 1999; Ordoñez and Pimentel, 2002; Vinasco et al., 2006; Weber et al., 2007; Cardona et al., 2008a; Ibañez-Mejía et al., 2008; Chew et al., 2008). However, in northernmost Colombia, paucity

* Corresponding author. Address: Smithsonian Tropical Research Institute, Ancón, Panama.
E-mail address: CardonaA@si.edu (A. Cardona).

0895-9811/$ - see front matter © 2010 Elsevier Ltd. All rights reserved.
doi:10.1016/j.jsames.2009.12.005

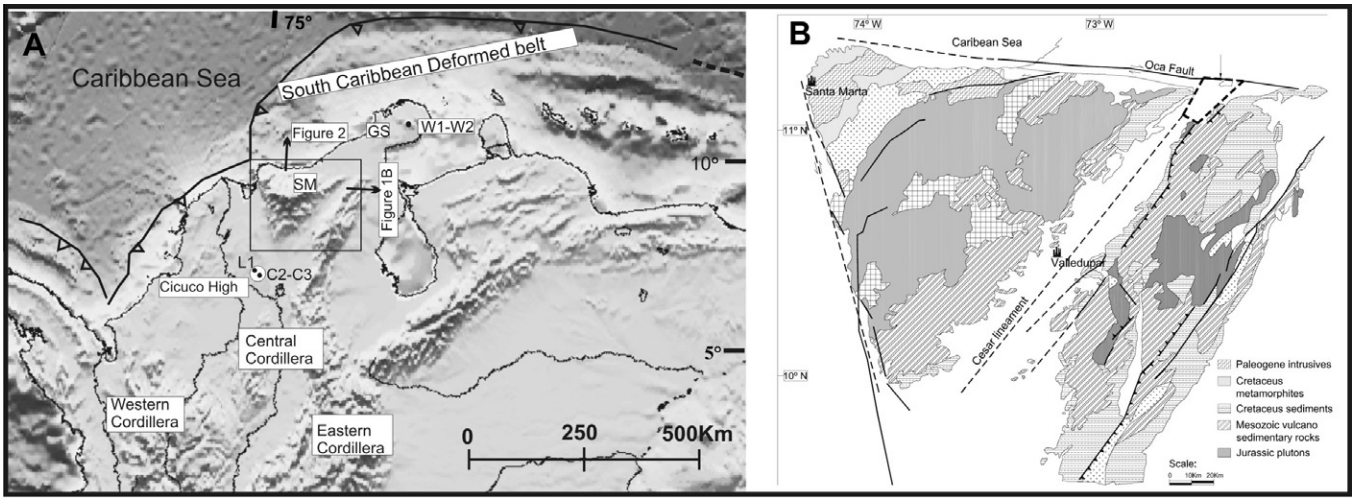

Fig. 1. (A) Digital elevation model of northern South America including major massifs and basins in northern Colombia. Triassic samples from the lower Magdalena basin and upper Guajira region from Montes et al. (2010) and Weber et al. (2010) are also plot. L1 = Lobita Well, C1 = Cicuco-1 Well, C2 = Cicuco-2 Well. W1 and W2 = samples collected in Guajira by Weber et al. (2010). (B) Geological map of the Sierra Nevada de Santa Marta (Tschanz et al., 1974).

of data, overimposed Meso-Cenozoic tectonic events and major sedimentary basins have limited the correlation of pre-Mesozoic crust with major Andean basement provinces and the understanding of the evolving collisional and/or accretionary orogens that have shaped the margins of Pangea.

In this contribution we integrate geologic, zircon U/Pb LAM-ICP-MS and whole rock geochemistry from mylonitized granitoids in the Sierra Nevada de Santa Marta massif with new geochemical data and recently published geochronological data obtained from the adjacent lower Magdalena basin (Montes et al., 2010) and the Guajira Peninsula (Weber et al., 2010) (Fig. 1A and B). It is argued that the regional distribution of this magmatism and the apparent shift in composition and deformation trace the regional tectonic and paleogeographic configuration of the margin (Pearce, 1996; Zhou et al., 2006). This segmented granitoid belt in northernmost Colombia has major implications in Pangean and Northern Andean tectonics.

2. Geological setting

The northern boundary of the Colombian Andes against the Caribbean plate is characterized by several isolated massifs bounded by Cenozoic basins and regional scale tectonic structures (Fig. 1). This physiographic configuration reflects the complex Late Mesozoic to Cenozoic tectonic interaction of the Caribbean, South American and Pacific plates, which has triggered block rotation, basin formation and tectonic uplift in northern Colombia (Kellogg, 1984; Macellari, 1995; Colletta et al., 1997; Taboada et al., 2000; Montes et al., 2005, 2010).

The Santa Marta Massif is a triangular uplifted segment located in northernmost Colombia that covers an area of 13.700 Km^2 and reaches altitudes of ~5.900 m. This massif can be divided into three different belts that is correlatable with other northern Andean domains as well as the adjacent northeastern Guajira Serranias (Fig. 1, reviews in Tschanz et al. (1974), Cordani et al. (2005), Cardona-Molina et al. (2006)). The southeasternmost belt includes a 1.0 Ga old high-grade metamorphic unit, that is part of a more extensive Grenvillian orogenic belt dispersed along the Colombian Andes, and records the ocean closure associated with the agglutination of Rodinia since ~1.25 Ga (Restrepo-Pace et al., 1997; Ruiz et al., 1999; Cordani et al., 2005). Jurassic plutonic and volcanic rocks intrude and cover this metamorphic unit, and are responsible for the segmentation. Minor Carboniferous and more widespread Late Mesozoic sedimentary sequences lie in unconformity towards the southeast flank (Tschanz et al., 1969, 1974; Rabe, 1977). The intermediate belt includes an intercalation of amphibole and mica-schists (Tschanz et al., 1969), and a newly recognized series of mylonitic granitoids in the northeast that will be described within this contribution. Previous temporal constrains from this unit limits depositional, magmatic and metamorphic evolution between the Late Cambrian and the Early Jurassic (Tschanz et al., 1974; Cardona-Molina et al., 2006). An overimposed greenschist facies mylonitic event has been related to the Late Cretaceous accretion of the Caribbean front (Tschanz et al., 1969; Cardona-Molina et al., 2006). The northwestenmost belt includes an imbricate stack of greenschist to amphibolite facies meta vulcano-sedimentary unit of Cretaceous age, related to the interaction of the front of the Caribbean plate with the northern margin of South America (MacDonald et al., 1971; Tschanz et al., 1974; Bustamante et al., 2009; Cardona et al., 2008a). Paleogene granitoids intrude the different belts and represent the stitching plutons of the Caribbean orogenic event (Tschanz et al., 1974; Cardona et al., 2008b). The lower Magdalena basin is a major Cenozoic tectonosedimentary element in northern Colombia. It is bounded by the Santa Marta Massif and the Santa Marta-Bucaramanga Fault to the east, and to the west it has been limited by the Romeral Fault System and the accreted oceanic San Jacinto belt. The foothills of the Central and Eastern Colombian Cordilleras enclose this basin. Its origin has been linked to northern Colombia block rotation associated to the post Eocene W–E migration of the Caribbean Plate and northern displacement of the North Andean block (Duque-Caro, 1978; Montes et al., 2010). Oil exploration wells and recent gravimetric modeling have shown that the substrate is made up of continental related magmatic and metamorphic rocks (Cerón et al., 2007). Basement rocks from this basin have been recovered in oil wells in the Cicuco High (Fig. 1A).

In this contribution we analyze a mylonitic granitoid segment in the Paleozoic segment of the Santa Marta Massif, and present new geochemical data from three granitoid cores recovered from the Cicuco-2A, Cicuco-3 and Lobita wells in the Cicuco High (Fig. 1A). Geocrhonological results from the latter are discussed by Montes et al. (2010).

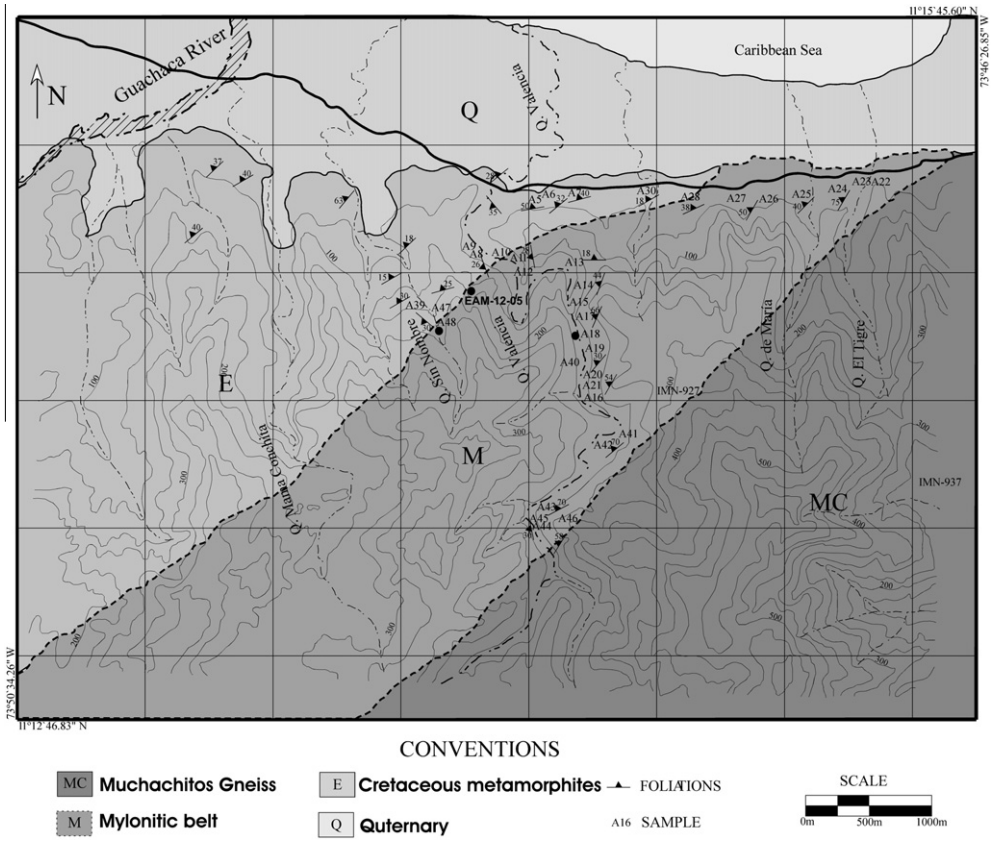

Fig. 2. Geology of the studied mylonitic zone (modified from Tschanz et al., 1974).

3. Analytical techniques

3.1. U/Pb LAM-ICP-MS

Zircon U/Pb analyses were carried at the Arizona LASERCHRON laboratoy following the procedures described by Valencia et al. (2005) and Gehrels et al. (2008). Unknowns and standard zircons were mounted in inner half of the mount area, to reduce fractionation. The grains analyzed were selected randomly from all of the zircons mounted from each sample. Zircons crystals were analyzed in polished section with a Micromass Isoprobe multicollector ICP-MS equipped with nine Faraday collectors, an axial Daly collector, and four ion-counting channels. The Isoprobe is equipped with an ArF Excimer laser ablation system, which has an emission wavelength of 193 nm. The collector configuration allows measurement of 204Pb in an ion-counting channel while 206Pb, 207Pb, 208Pb, 232Th and 238U are simultaneously measured with Faraday detectors. All analyses were conducted in static mode with a laser beam diameter of 35–50 diameter, operated with an output energy of ~32 mJ (at 23 kV) and a pulse rate of 9 Hz. Each analysis consisted of one 20-s integration on peaks with no laser firing and twenty 1-s integrations on peaks with the laser firing. Hg contribution to the 204Pb mass position was removed by subtracting on-peak background values. Inter-element fractionation was monitored by analyzing an in-house zircon standard, which has a concordant TIMS age of 564 ± 4 Ma (2σ) (Gehrels, unpublished data). This standard was analyzed once for every four unknowns in magmatic grains. Uranium and Th concentrations were monitored by analyzing a standard (NIST 610 Glass) with ~500 ppm Th and U. The lead isotopic ratios were corrected for common Pb, using the measured ^{204}Pb, assuming an initial Pb composition according to Stacey and Kramers (1975) and respective uncertainties of 1.0, 0.3 and 2.0 for ^{206}Pb/^{204}Pb, ^{207}Pb/^{204}Pb, and ^{208}Pb/^{204}Pb.

Age of standard, calibration correction from standard, composition of common Pb and decay constant uncertainty are grouped and are known as the systematic error. For these samples the systematic errors are around ~1.0–1.4% for ^{206}Pb/^{238}U and ~0.8–1.1 for ^{206}Pb/^{207}Pb.

3.2. Whole rock geochemistry

Whole rock chemical analyses of 10 samples were determined at Acme Analytical Laboratories Ltd. in Vancouver, Canada. A 0.2 g aliquot is weighed into a graphite crucible and mixed with

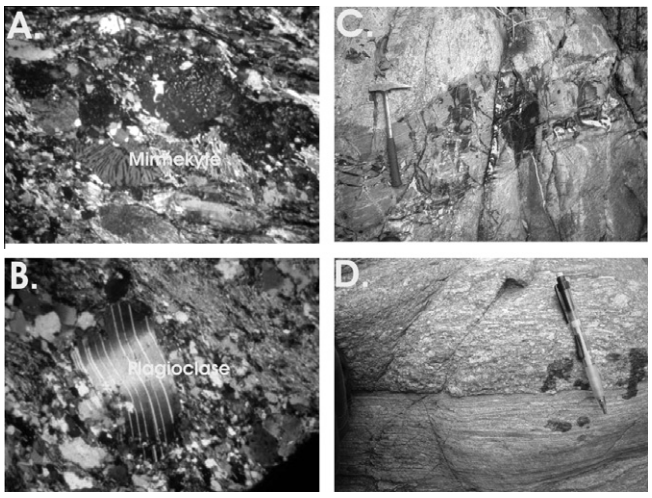

Fig. 3. Amphibolite xenolith in deformed granitoid (Quebrada Valencia). Myrmekite and kinked plagioclase deformation textures.

Table 1
U/Pb zircon analytical results.

Analysis	U (ppm)	206Pb 204Pb	U/Th	207Pb* 235U	± (%)	206Pb* 238U	± (%)	Error Corr.	206Pb* 238U	± (Ma)	207Pb* 235U	± (Ma)	206Pb* 207Pb*	± (Ma)	Best age (Ma)	± (Ma)
A14-4	968	11410	0.8	0.32966	1.5	0.04575	1.0	0.68	288.4	2.8	289.3	3.7	296.6	24.6	288.4	2.8
A14-5	917	10377	0.9	0.31984	1.6	0.04463	1.0	0.61	281.5	2.8	281.8	4.0	284.5	29.7	281.5	2.8
A14-6	548	9486	1.3	0.33109	3.2	0.04573	1.1	0.34	288.3	3.1	290.4	8.1	307.5	68.3	288.3	3.1
A14-7	586	2967	1.2	0.3205	5.1	0.04383	3.7	0.72	276.5	9.9	282.3	12.5	330.4	79.1	276.5	9.9
A14-8	784	4998	1.1	0.31542	4.6	0.04477	2.8	0.60	282.3	7.6	278.4	11.1	245.1	83.9	282.3	7.6
A14-9	971	8361	2.1	0.31019	2.6	0.04395	1.1	0.40	277.2	2.9	274.3	6.3	249.5	55.5	277.2	2.9
A14-10A	690	6084	2.3	0.32598	3.8	0.0451	1.7	0.45	284.4	4.7	286.5	9.5	303.9	77.6	284.4	4.7
A14-11	800	19179	1	0.33105	2.0	0.04629	1.0	0.50	291.7	2.9	290.4	5.0	279.5	39.2	291.7	2.9
A14-12	623	11368	1.1	0.32788	1.9	0.04585	1.0	0.53	289.0	2.8	287.9	4.8	279.5	37.0	289.0	2.8
A14-13	759	9153	0.9	0.31571	3.2	0.04517	1.3	0.41	284.8	3.7	278.6	7.8	227.1	67.5	284.8	3.7
A14-15	629	10417	1.2	0.33737	4.2	0.04595	1.1	0.26	289.6	3.1	295.2	10.8	339.3	92.1	289.6	3.1
A14-15a	818	22419	1	0.33582	1.5	0.04658	1.0	0.68	293.5	2.9	294.0	3.8	298.0	24.8	293.5	2.9
A14-16	1015	17326	0.8	0.31669	3.1	0.04496	1.7	0.57	283.5	4.8	279.4	7.5	244.5	57.7	283.5	4.8
A14-17	636	5451	0.7	0.33517	2.9	0.04694	2.1	0.73	295.7	6.1	293.5	7.4	276.2	45.5	295.7	6.1
A14-18	666	9955	0.6	0.33093	2.7	0.0467	1.6	0.60	294.3	4.6	290.3	6.7	258.3	48.8	294.3	4.6
A14-21	655	10400	1.4	0.31513	2.8	0.04503	1.0	0.35	283.9	2.8	278.1	6.9	229.8	61.1	283.9	2.8
A14-23	818	14274	1.7	0.33574	3.0	0.04635	1.0	0.33	292.0	2.9	293.9	7.7	309.0	65.3	292.0	2.9
A14-25	844	10719	1	0.3281	2.4	0.0458	1.9	0.80	288.7	5.4	288.1	6.0	283.7	33.3	288.7	5.4
A14-26	768	8924	1.1	0.31618	4.8	0.04486	3.5	0.73	282.9	9.8	279.0	11.8	246.3	75.7	282.9	9.8
A14-27	688	3176	1	0.31413	6.0	0.045	3.1	0.51	283.8	8.5	277.4	14.5	223.9	118.6	283.8	8.5
A14-28	985	19425	0.6	0.31784	4.1	0.04455	3.9	0.95	280.9	10.8	280.2	10.1	274.4	28.4	280.9	10.8
A14-29	962	16702	1.1	0.31751	2.4	0.04404	2.0	0.81	277.8	5.4	280.0	5.9	298.0	32.1	277.8	5.4
A14-31	551	8291	0.9	0.33205	2.8	0.04508	2.3	0.81	284.2	6.3	291.1	7.1	347.0	36.8	284.2	6.3
A14-32	465	10946	0.8	0.34407	4.0	0.04697	2.2	0.56	295.9	6.5	300.3	10.5	334.3	76.2	295.9	6.5
A14-33	632	9471	0.9	0.32124	2.0	0.04538	1.4	0.69	286.1	3.9	282.9	5.0	256.0	33.9	286.1	3.9
A14-35	662	9961	0.7	0.3555	3.5	0.04707	2.8	0.78	296.5	8.0	308.8	9.4	402.8	48.8	296.5	8.0
A14-36	845	11900	3.2	0.33527	4.0	0.0451	1.5	0.37	284.3	4.1	293.6	10.2	367.7	84.2	284.3	4.1
A14-37	411	5637	1.7	0.34622	3.3	0.04674	2.1	0.65	294.5	6.1	301.9	8.5	359.4	56.2	294.5	6.1
A14-38	525	3760	1.1	0.34941	5.4	0.04706	2.4	0.45	296.4	6.9	304.3	14.1	364.8	108.4	296.4	6.9
A14-39	398	6633	1.3	0.32163	5.8	0.04568	5.3	0.91	288.0	14.8	283.2	14.3	243.7	55.5	288.0	14.8
A14-40	579	9585	1.3	0.32656	1.6	0.04554	1.1	0.67	287.1	3.1	286.9	4.1	285.9	28.0	287.1	3.1
A14-41	590	7480	1.7	0.32598	3.8	0.04617	1.8	0.47	291.0	5.1	286.5	9.5	250.1	77.4	291.0	5.1
A14-43	604	9179	1.3	0.31817	3.1	0.04497	2.8	0.90	283.5	7.7	280.5	7.6	255.1	31.5	283.5	7.7
A14-44	604	11810	1.2	0.32809	2.0	0.04582	1.4	0.69	288.8	3.9	288.1	5.1	282.5	33.6	288.8	3.9
A14-46	777	11483	1.2	0.32399	3.1	0.04579	1.4	0.45	288.6	4.0	285.0	7.8	254.9	64.5	288.6	4.0
A14-47	422	2740	1.3	0.32476	9.0	0.04524	4.1	0.45	285.2	11.3	285.6	22.4	288.3	183.4	285.2	11.3
A14-48	736	22471	2.1	0.34119	8.4	0.0461	1.8	0.21	290.6	5.1	298.1	21.8	357.4	186.4	290.6	5.1
A14-51	773	21614	1	0.33653	2.9	0.0466	1.1	0.38	293.6	3.2	294.5	7.5	302.1	61.6	293.6	3.2
A14-53	962	10404	0.9	0.32707	2.1	0.04586	1.2	0.55	289.1	3.3	287.3	5.3	273.3	40.6	289.1	3.3
A14-55	1069	15988	2	0.33187	2.4	0.0459	1.1	0.47	289.3	3.2	291.0	6.0	304.4	47.9	289.3	3.2
A14-56	720	7011	1.2	0.31652	5.1	0.0452	2.7	0.53	285.0	7.6	279.2	12.5	231.2	100.7	285.0	7.6
A14-57	548	7941	1.5	0.33461	3.9	0.04588	2.7	0.69	289.2	7.6	293.1	10.0	324.3	64.6	289.2	7.6
A14-58	924	12886	2.3	0.31671	2.8	0.04385	1.1	0.41	276.6	3.1	279.4	6.9	302.2	58.7	276.6	3.1
A14-60A	647	13154	1.3	0.31637	4.2	0.04447	1.5	0.36	280.5	4.2	279.1	10.2	267.6	88.9	280.5	4.2
A14-61	649	6586	1.4	0.31405	4.3	0.04411	2.9	0.68	278.3	7.8	277.3	10.3	269.2	71.8	278.3	7.8
A14-62	554	8377	1.9	0.33558	4.7	0.04508	2.1	0.45	284.2	5.9	293.8	12.1	370.8	95.7	284.2	5.9
A14-63	730	18717	0.9	0.33643	3.7	0.04623	3.0	0.81	291.4	8.4	294.5	9.3	319.2	48.9	291.4	8.4
A14-65	639	8487	1.3	0.32946	5.1	0.04548	2.8	0.54	286.7	7.8	289.2	12.9	309.0	98.3	286.7	7.8
A14-69	865	16580	0.7	0.3251	2.2	0.04544	2.0	0.88	286.4	5.5	285.8	5.5	280.7	23.8	286.4	5.5
A14-1	216	11734	2.2	1.17261	5.0	0.13225	4.3	0.86	800.7	32.2	787.9	27.4	751.8	54.5	800.7	32.2
A14-66	266	6215	1	1.31672	2.7	0.11999	1.5	0.54	730.5	10.1	853.1	15.6	1186.8	44.7	730.5	10.1
A14-49	1644	68190	20.1	0.83293	3.0	0.10024	1.9	0.62	615.8	11.1	615.2	14.0	613.1	51.2	615.8	11.1
A14-60	416	25409	2.4	2.29115	4.3	0.20631	2.4	0.56	1209.1	26.3	1209.6	30.2	1210.3	69.8	1210.3	69.8
A48-05	491	8196	1.2	0.33066	1.6	0.04541	1.0	0.62	286.3	2.8	290.1	4.1	320.5	28.9	286.3	2.8
A48-06	481	5527	1.2	0.30298	3.0	0.04304	1.0	0.33	271.6	2.7	268.7	7.1	243.5	65.1	271.6	2.7
A48-07	747	1766	1.4	0.54101	4.0	0.04449	1.6	0.41	280.6	4.5	439.1	14.3	1386.7	70.5	280.6	4.5
A48-08	522	5628	1.5	0.31003	8.2	0.04218	3.6	0.43	266.3	9.3	274.2	19.8	342.0	168.4	266.3	9.3
A48-09	205	3603	1.8	0.32982	2.3	0.04395	1.0	0.43	277.3	2.7	289.4	5.8	388.9	46.9	277.3	2.7
A48-10	775	2542	2.1	0.33584	4.1	0.04256	1.8	0.45	268.7	4.8	294.0	10.5	500.4	81.1	268.7	4.8
A48-11	339	4038	2	0.318	5.2	0.04348	2.4	0.46	274.4	6.3	280.4	12.7	330.6	104.5	274.4	6.3
A48-12	467	1351	1.9	0.30631	5.9	0.04453	3.5	0.59	280.8	9.6	271.3	14.1	189.8	111.0	280.8	9.6
A48-13	164	1684	1.7	0.31482	13.5	0.0436	2.8	0.21	275.1	7.7	277.9	32.7	301.4	301.1	275.1	7.7
A48-14	824	6056	1.5	0.29212	3.9	0.04134	2.5	0.65	261.2	6.5	260.2	9.0	251.8	69.1	261.2	6.5
A48-15	304	6497	1.4	0.32586	3.5	0.04493	2.5	0.72	283.3	7.0	286.4	8.8	311.8	55.6	283.3	7.0
A48-17	463	7869	1.7	0.30412	3.7	0.04222	2.4	0.65	266.6	6.2	269.6	8.7	296.2	63.8	266.6	6.2
A48-19	937	4066	1.9	0.3407	5.2	0.04468	1.7	0.33	281.8	4.8	297.7	13.4	424.4	109.6	281.8	4.8
A48-20	400	1789	0.9	0.31092	3.4	0.04399	1.3	0.39	277.5	3.6	274.9	8.2	252.8	72.4	277.5	3.6
A48-21	1890	19243	1.3	0.31187	2.0	0.04344	1.2	0.60	274.1	3.2	275.6	4.7	288.4	35.9	274.1	3.2
A48-23	758	6671	1.9	0.32498	5.6	0.04501	4.2	0.74	283.8	11.6	285.7	14.1	301.6	86.8	283.8	11.6
A48-24	665	10043	1.7	0.31602	4.5	0.04294	3.1	0.68	271.0	8.1	278.8	11.0	344.8	74.9	271.0	8.1
A48-25	344	7325	1.9	0.31912	3.4	0.04318	2.9	0.85	272.5	7.8	281.2	8.4	354.3	40.6	272.5	7.8
A48-26	79	1797	2	0.31229	4.1	0.04324	3.1	0.76	272.9	8.4	276.0	10.0	302.2	60.6	272.9	8.4
A48-27	205	1245	2.3	0.31361	7.6	0.04336	6.0	0.79	273.6	16.0	277.0	18.4	305.5	106.9	273.6	16.0

(*continued on next page*)

Table 1 (*continued*)

Analysis	U (ppm)	206Pb 204Pb	U/Th	207Pb* 235U	± (%)	206Pb* 238U	± (%)	Error Corr.	206Pb* 238U	± (Ma)	207Pb* 235U	± (Ma)	206Pb* 207Pb*	± (Ma)	Best age (Ma)	± (Ma)
A48-28	155	2960	1.6	0.31096	4.9	0.04293	3.9	0.79	270.9	10.4	274.9	11.9	308.9	68.4	270.9	10.4
A48-29	1068	13506	1.6	0.32621	3.5	0.04307	1.4	0.41	271.8	3.8	286.7	8.8	409.5	72.4	271.8	3.8
A48-3	2094	5039	1.1	0.28296	5.5	0.03999	4.6	0.83	252.7	11.3	253.0	12.4	255.3	71.6	252.7	11.3
A48-30	352	5660	1.6	0.31682	5.3	0.04303	2.7	0.52	271.6	7.3	279.5	13.0	345.6	102.9	271.6	7.3
A48-31	318	4589	1.9	0.33019	4.7	0.04462	3.9	0.82	281.4	10.7	289.7	11.9	357.2	60.8	281.4	10.7
A48-32	513	16420	1.9	0.34143	2.5	0.0444	1.9	0.75	280.1	5.2	298.3	6.5	443.1	37.2	280.1	5.2
A48-33	420	789	2	0.28396	7.2	0.04158	3.4	0.48	262.6	8.8	253.8	16.1	173.0	146.9	262.6	8.8
A48-34	295	5626	2.1	0.31559	4.0	0.04319	3.4	0.85	272.6	9.0	278.5	9.7	328.4	47.7	272.6	9.0
A48-35	243	1283	1.7	0.32614	5.0	0.04444	2.4	0.48	280.3	6.7	286.6	12.6	338.2	99.8	280.3	6.7
A48-36	505	5910	2	0.3203	2.3	0.04383	1.7	0.76	276.5	4.7	282.1	5.6	328.8	33.6	276.5	4.7
A48-37	685	10047	1.6	0.30717	2.5	0.04333	1.7	0.69	273.4	4.7	272.0	6.0	259.6	42.1	273.4	4.7
A48-39	1034	17659	3	0.34087	2.6	0.04539	1.8	0.70	286.2	5.1	297.8	6.6	390.2	41.1	286.2	5.1
A48-4	342	2284	1	0.31663	3.1	0.04431	2.1	0.67	279.5	5.7	279.3	7.6	277.5	52.7	279.5	5.7
A48-40	1649	1686	1.7	0.36948	2.8	0.04316	1.0	0.36	272.4	2.7	319.3	7.7	676.9	55.9	272.4	2.7
A48-41	379	7040	1.5	0.30361	4.0	0.04154	1.8	0.44	262.3	4.5	269.2	9.4	329.4	81.2	262.3	4.5
A48-42	212	4545	1.8	0.33708	4.3	0.04574	2.1	0.48	288.3	5.9	295.0	11.0	347.9	85.2	288.3	5.9
A48-44	260	6783	1.9	0.32165	2.6	0.04391	1.0	0.39	277.0	2.7	283.2	6.4	334.1	53.9	277.0	2.7
A48-45	179	1458	1.8	0.31874	4.8	0.04249	1.8	0.38	268.3	4.8	280.9	11.7	387.7	99.1	268.3	4.8
A48-46	345	4774	1.9	0.30736	2.4	0.04362	1.9	0.80	275.2	5.1	272.1	5.7	245.4	33.3	275.2	5.1
A48-47	509	5227	2	0.32748	3.5	0.04444	2.3	0.66	280.3	6.3	287.6	8.7	347.6	59.0	280.3	6.3
A48-48	1035	1137	4.8	0.31182	9.0	0.04431	6.0	0.66	279.5	16.3	275.6	21.8	242.7	156.3	279.5	16.3
A48-49	296	5741	2	0.31702	2.5	0.04333	1.7	0.66	273.4	4.5	279.6	6.2	331.7	43.4	273.4	4.5
A48-50	371	2501	1.3	0.32003	3.8	0.04491	1.6	0.43	283.2	4.5	281.9	9.4	271.4	79.3	283.2	4.5
A48-51	381	6167	1.3	0.36067	4.0	0.04382	1.2	0.31	276.5	3.3	312.7	10.6	592.5	81.5	276.5	3.3
A48-52	923	12506	2	0.34732	3.2	0.04696	2.5	0.79	295.9	7.3	302.7	8.4	355.9	44.2	295.9	7.3
A48-53	690	918	2.6	0.32044	8.4	0.04606	3.3	0.40	290.3	9.5	282.2	20.6	216.0	178.1	290.3	9.5
A48-54	841	12400	1.4	0.32511	3.0	0.04493	2.5	0.82	283.3	6.9	285.8	7.6	306.6	39.1	283.3	6.9
A48-55	382	4960	1.5	0.33811	2.7	0.04528	1.3	0.46	285.5	3.5	295.7	7.0	377.4	54.5	285.5	3.5
A48-57	908	2132	1.1	0.33629	4.0	0.04595	2.3	0.58	289.6	6.6	294.4	10.3	332.3	74.6	289.6	6.6
A48-58	984	15833	1.4	0.30932	2.0	0.04334	1.4	0.68	273.5	3.7	273.7	4.9	275.0	34.5	273.5	3.7
A48-60	477	5337	1.4	0.30527	4.5	0.04331	2.8	0.62	273.3	7.6	270.5	10.8	246.1	81.7	273.3	7.6

1.5 g of $LiBO_2$ flux. The crucibles are placed in an oven and heated to 1050 °C for 15 min. The molten sample is dissolved in 5% HNO_3. Calibration standards and reagent blanks are added to the sample sequence. Sample solutions are aspirated into an ICP emission spectrograph (Jarrel Ash Atom Comb 975) for determining major oxides and certain trace elements (Ba, Nb, Ni, Sr, Sc, Y and Zr), while the sample solutions are aspirated into an ICP-MS (Perkins–Elmer Elan 6000) for determination of the trace elements, including rare earth elements.

3.3. Mineral chemistry

Biotite compositions were obtained by wavelength-dispersive spectrometry (WDS) with a Cameca SX-50 microprobe (University of Granada), operated at 20 kV and 20 nA, and synthetic SiO_2, Al_2O_3, $MnTiO_3$, Fe_2O_3, MgO and natural diopside, Albite and sanidine as calibration standards.

4. Field and petrologic relations

Tschanz et al. (1969, 1974) defined the Sevilla Province within the Santa Marta Massif as a major SW–NE Paleozoic metamorphic belt. These authors divided it into the Buritaca Gneiss, composed mainly of hornblende gneisses, amphibolites and some migmatites, and the Los Muchachitos Gneiss comprising similar rocks, but including intercalations of two mica-schists and marbles. A major retrograde greenschist facies deformational event has been considered as one of the more peculiar features of the Los Muchachitos Gneiss (Tschanz et al., 1969). Based on structural relations and a ca. 250 Ma K–Ar age (MacDonald and Hurley, 1969) from a deformed granitoid clast found in the Don Diego River, these authors considered the existence of an orthogneiss of Late Permian age that may be linked to this belt.

During recent field work carried out in the northeastern coastal region, a major shear zone with a SW–NE trend and ca. 6 km of extension was identified (Fig. 2). Protoliths of this mylonitic belt are hornblende-biotie schists from the Los Muchachitos Gneiss and a prominent quartzofeldspathic unit. To the southwest non-mylonitic amphibole schists also related to the Paleozoic Los Muchachitos Gneiss were found, whereas to the northwest two mica-schists related to the meta volcano-sedimentary Cretaceous unit are exposed. The contact between this Cretaceous metamorphic rocks and the Paleozoic belt coincides with the major mylonic belt, and represent a paleogeographic limit between allocthonous accreted Caribbean elements and continental basement.

Mylonitic folitation follows a SW–NE trend, dipping between 30° and 70° to the NW, with shallow dipping mineral lineation (10–30° NE). Mica fish and quarter folds were found as dextral kinematic indicators.

The quartzofeldespatic unit includes mylonites and protomylonites, with relict K Feldspar (5–40%), Plagioclase (10–40%) and Biotite (<5%) porphyroclasts, sourronded by a matrix formed during deformation by the crystallization of Muscovite (5–25%) + Biotite (10–30%) + Quartz (20–40%) + Epidote (3–20%) + Chlorite + titanite. Accessory primary minerals include zircon, titanite, apatite and opaques. The main deformational fabric is characterized by Quartz with ondulatory extinction, deformation llamellae and grain boundary migration, whereas feldspar is microfractured and also shows ondulatory extinction. Plagioclase kinks and oriented myrmekites are surrounded by this finer-grained matrix of mica and Quartz (Fig. 3A and B), attesting to a previous deformational recrystallization. Structures related to a magmatic origin include porphyritc idiomorphic feldspars (Fig. 3C), deformed aplitic dikes and both magmatic and metamorphic enclaves (Fig. 3D). Perthite and graphic microtextures are also considered as magmatic remnants. Variable proportions of feldspar porphyroclasts, the anorthite content between An_{36}–$An_{52,}$ and the compositional variation in the neoformed minerals of the matrix are most likely

related to a compositional variability from the magmatic precursor. Relict titanite and apatite suggest an I-type origin (Barbarin, 1999) for the protolith granitoid. The presence of amphibole schist xenoliths (Fig. 3C) indicates that the contact between the granitoid and the metamorphic rocks of the Los Muchachitos Gneiss is intrusive. Relations with the northwestern schist belt are not well defined, and no intrusive contacts were seen in the field.

The amphibole schists from Los Muchachitos Gneiss show an amphibolite facies foliation defined by Hornblende + Plagioclase (An_{52}) + Biotite + Qartz with titanite, apatite and opaques as accessory minerals. A retrograde mylonitic overprint with a spaced cleavage defined by Epidote + Biotite + Chlorite + Quartz. The schist belt is made up of fine to medium grained mica schist with minor intercalation of marbles and quartz-actinolite schists. The principal foliation on this unit is defined by Muscovite + Biotite + Quartz ± Chlorite and Actinolite + Albite + Chlorite + Epidote, and follows the same trend seen in the mylonitic belt.

4.1. Cicuco High granitoids

Granitoid cores recovered from the Cicuco High industry wells have been described by Montes et al. (2010). We have analyzed the same samples from the Cicuco-2a, Cicuco-3 and Lobita-1 wells in the Cicuco High (Fig. 1). Location and basement depths are as follow: Cicuco-2a (74°38′53.07″W, 9°16′24.781″N, 2,4 km deep), Cicuco-3 (−74°38′51.94″W, 9°17′38.58″, 2,5 km deep) and Lobita-1 (−74°41′30.83″, 9°18′30″, 2.5 km deep). The rocks are two mica granites, with average Quartz (55%), K-feldspar (15%), plagioclase (18%), Biotite (6%) and Muscovite (6%), and include an overprint greenschist facies deformation (Montes et al., 2010).

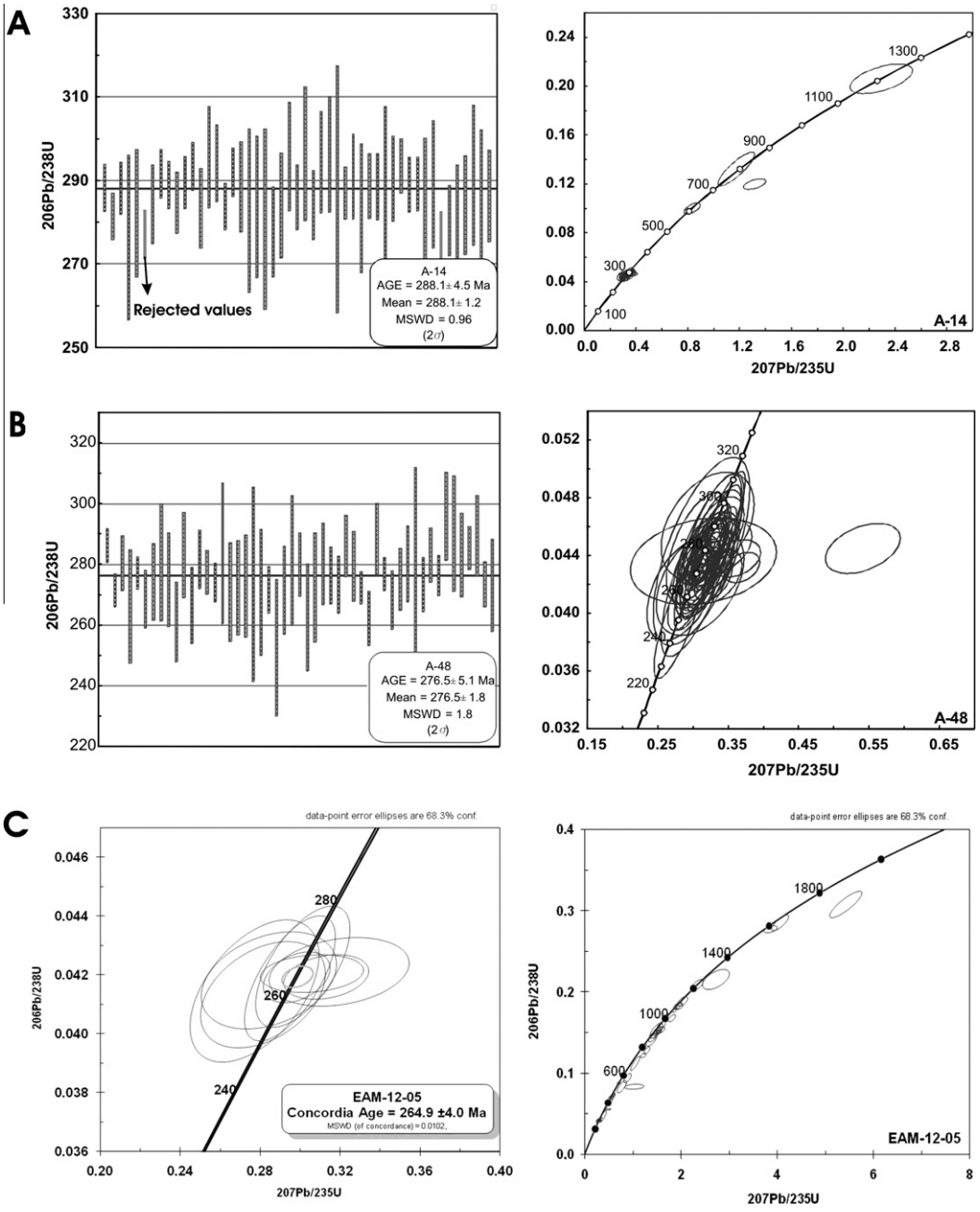

Fig. 4. U/Pb geochronological results from mylonitic granitoids: (A) Sample A14, (B) Sample A48 and (C) Sample EAM-12-05.

Table 2
Whole rock geochemical data from the mylonitic granitoids.

Sample	SiO_2	Al_2O_3	Fe_2O_3	MgO	CaO	Na_2O	K_2O	TiO_2	P_2O_5	MnO	Cr_2O_3	LOI	Total	Ba	Co	Cs	Hf	Nb	Rb	Sr	Ta	Th	U	V	Zr	Y	Pb	Ni	Sc	La	Ce	Pr	Nd	Sm	Eu	Gd	Tb	Dy	Ho	Er	Tm	Yb	Lu
A11	59.05	16.84	6.44	3.03	4.27	4.19	3	0.88	0.29	0.11	0.006	1.6	99.71	746.1	14.6	2.2	5.2	15.7	107.7	560	1.4	18.5	3.5	147	176	30.9	2.3	10.7	16	30.4	79.8	10.18	40.4	7.42	1.54	5.75	0.95	5.05	0.94	2.72	0.43	2.63	0.36
A12	58.87	17.6	7.69	0.98	5.48	3.8	2.77	0.79	0.32	0.16	0.002	1.5	99.97	790.6	6.5	2.7	5.3	20.1	92.5	763.5	1.1	23.7	5.5	101	219.6	29.1	4.7	9.8	8	30.6	70.5	8.48	33.3	6.69	1.85	5.17	0.89	4.37	0.87	2.63	0.39	2.81	0.44
A13	76.26	11.83	2.9	0.95	1.58	2.9	1.88	0.39	0.05	0.06	0.013	0.9	99.72	1029	5.8	2.4	5.8	8.3	67.6	285.8	0.6	16.5	1.9	51	197.8	9.1	12	13.7	6	33.7	73.2	8.13	28.6	4.62	0.98	2.93	0.45	1.78	0.31	0.75	0.12	0.76	0.14
A15	65.82	15.91	4.09	1.16	3.71	4.09	3.37	0.54	0.19	0.11	0.002	1	99.99	1052.3	6.9	1.7	5.5	25.2	90.8	694.1	1.4	21	5.9	68	199.4	23.1	.	4.3	6	36.1	74.3	7.85	27.9	5.1	1.37	3.91	0.66	3.31	0.65	2.04	0.33	2.21	0.35
A16	61.85	16.09	5.6	1.73	3.68	2.94	4.22	1.11	0.66	0.08	0.007	1.7	99.67	1321.9	9.1	1.6	7.4	18.3	128.4	362.1	0.8	2.9	1	70	281.7	24.6	5	11.4	9	59.6	149	19.46	80.6	14.13	2.04	9.82	1.22	5.17	0.77	2.02	0.22	1.32	0.18
A21	63.38	16.71	4.13	1.35	4.41	4.48	2.65	0.55	0.23	0.1	0.004	1.7	99.7	841.4	5.9	2.5	5.6	24	97.4	757.9	1.8	24	3.8	75	200	24	3.9	7.4	6	38.8	78.4	8.48	31.4	5.81	1.48	4.51	0.76	3.83	0.73	2.3	0.32	2.28	0.35
A24	65.05	14.68	7.25	2.09	1.14	1.41	3.76	0.73	0.18	0.09	0.011	3.7	100.1	639.2	12.9	2.2	5	16	109.2	123.9	1.1	15.2	4	108	183.6	33.2	11.4	40	14	35.1	78.3	9.16	34.6	6.62	1.46	5.73	1.07	5.13	0.97	2.95	0.41	2.94	0.43
A26	65.87	15.83	4.21	1.06	2.88	3.64	3.58	0.52	0.19	0.09	0.003	1.8	99.68	1205.4	6.4	1.5	5.3	23.9	105.3	575.7	1.8	18.7	4.3	72	178.6	22.7	3.3	4.3	6	28.3	64	7.29	27.7	5.08	1.25	4.31	0.72	3.74	0.7	2.16	0.32	2.15	0.35
A43	71	15.65	3.06	0.44	2.92	5.36	0.98	0.23	0.07	0.03	0.002	0.1	99.83	1650.7	3.1	0.2	2.3	1.6	13.1	723.9		0.3	0.1	16	104.5	2.3	1	9.7	1	3.5	6.6	0.73	2.5	0.42	0.55	0.35	0.06	0.29	0.07	0.21	0.04	0.24	0.05
A44	70.01	16.16	1.87	0.31	2.52	4.87	2.73	0.19	0.06	0.09	0.002	0.9	99.71	1052.7	1.3	0.4	3.3	7.7	43	674.1	0.6	2.1	1.7	22	82.7	9.2	1.9	1.1	2	7.8	16.6	1.98	8.4	1.63	0.59	1.47	0.27	1.33	0.25	0.78	0.14	0.96	0.16
A46	72.64	15.64	1.47	0.3	2.72	5.35	0.8	0.18	0.03	0.02		0.7	99.84	1512.5	1.6	0.2	2.7	1.4	10.5	706.6			0.1	10	103.8	1.2	0.9	3.4	1	1.3	2.2	0.23	1.1	0.17	0.65	0.19	0.02	0.14	0.03	0.12	0.02	0.18	0.04
CICUCO 2A	68.39	14.86	4.78	1.55	2.13	2.74	2.83	0.52	0.174	0.07		1.8	99.83	577	7.4	1.7	6	13.5	92.9	179.7	1	15.4	3.9	61	195.4	34.7	10.5	28	9	31.4	67.4	8.6	33.2	7	0.89	6.18	1.07	5.86	1.18	3.22	0.48	2.98	0.43
CICUCO 3	68.74	15.2	3.49	1.06	1.57	2.89	4.01	0.45	0.156	0.05		2.2	99.8	930	6.1	2.1	4.9	10.7	120.9	178	1	12.9	3.3	52	166.1	31.3	8.8	22	7	25.9	53.9	6.92	28.7	5.61	1.07	5.32	0.94	5.18	1.09	2.99	0.43	2.89	0.41
LOBITA 1	69.39	14.89	4.11	1.25	1.23	2.52	3.34	0.56	0.182	0.05		2.3	99.85	448		3.7	6.7	14.2	137.9	124.8	1.0	17.4	5.9		222.9	32.4				32.5	70.8	8.9	37	6.92	5.61	0.96	6.64	1.09	5.93	1.16	2.95	0.42	2.71	0.37

4.2. U/Pb geochronology

Two granitoid samples from Santa Marta mylonites were selected for zircon U/Pb LAM-ICP-MS geochronological analyses. In some of the samples we chose to analyze a broader amount of zircon crystals in order to identify the magmatic age, but also possible xenocrystal or inherited ages that will shed a light in the existence of assimilated material during magma genesis and the nature of the crustal domain where the magma was formed.

Analytical data is presented in Table 1 and concordia plots are shown in Fig. 4. All zircons from both samples present U/Th ratios <12 that can be related to a growth within magmatic conditions (Rubatto, 2002).

All except one of the 52 zircons from sample A14 plot along the concordia, four zircons yield 615 ± 11 Ma, 730 ± 10 Ma, 800 ± 32 Ma, 1210 ± 69 Ma that are related to inherited zircons that record the character of the crystal domain were this rock was formed. The other 48 crystals yield a weight average $^{206}Pb/^{238}U$ age with its associated propagation error of 288.1 ± 4.5 Ma (Fig. 4A). This age is related to the Early Permian magmatic crystallization of the granitoid. Zircons from sample A48 are concordant, and have yielded a weighted average age $^{206}Pb/^{238}U$ of 276.5 ± 5.1 Ma (Fig. 4B).

There seems to be a trend towards younger Late Permian ca. 250 Ma ages with some ages in sample A48 slightly younger, that are probably related to a Pb-loss event. Zircons from sample EAM-12-05 are characterized by a significant amount of inherited zircons with Early Paleozoic and Grenvillian ages. Nine zircon tips from this mylonite have yielded an $^{206}Pb/^{238}U$ of 264.9 ± 4.0 Ma age (Fig. 4C) which also records the crystallization of the magmatic precursor.

4.3. Geochemistry

Major and trace elements whole rock analysis for the granitoid mylonite samples and three granitoids cores recovered from the Cicuco-1, Cicuco-2a and the Lobita-1 wells of the Cicuco High analyzed by Montes et al. (2010) are presented in Table 2. Due to recrystallization and deformation associated with the metamorphic overprint, large ion lithophile elements were probably mobilized and their meaning is interpreted with caution. In contrast, the relatively immobile behaviour of HFSE and REE are meaningful for petrogenetic interpretations (Michard, 1989; Wilson, 1989; Rollinson, 1993, Hollings and Wymann, 2005). SiO_2 and Al_2O_3 contents for the mylonites are moderate to high, varying between 58.8% and 72.6% and 11.8–17.6 wt.% respectively. The Cicuco High granitoids present higher silica and aluminium values (68.3–69.3 wt.%, 14.82–15.3 wt.%). Selected major and trace elements for the mylonites were plotted against silica in Harker-type diagrams. Although some dispersion is commonly seen, general negative trends for TiO_2, MgO, Al_2O_3, MnO and P_2O_5 (Fig. 5) reflect precursor magmatic processes. As expected the highly mobile K_2O and Na_2O are more scattered possibly linked to element mobility during deformation. Some trace elements such as Sc and V also show a coherent negative correlation with SiO_2 (Fig 5). Within an Al_2O_3 versus MgO protolith discrimination diagram (Marc, 1992), all the samples from the mylonitic granitoid fall in the orthogneiss field (Fig. 6), re-inforcing their magmatic origin suggested by field and textural observations.

Within a TAS classification diagram the rocks are classified as syenodiorite, granodiorite and granite (Fig. 7A), and within the SiO_2-(Zr/TiO_2) diagram after Winchester and Floyd (1977), the granitoid samples plot in a continuous trend that may be related to plutonic equivalents of andesite to rhyolite (Fig. 7B). The Cicuco granitoids are also felsic, falling within fields comparable with the Santa Marta mylonites (Fig. 7A and B).

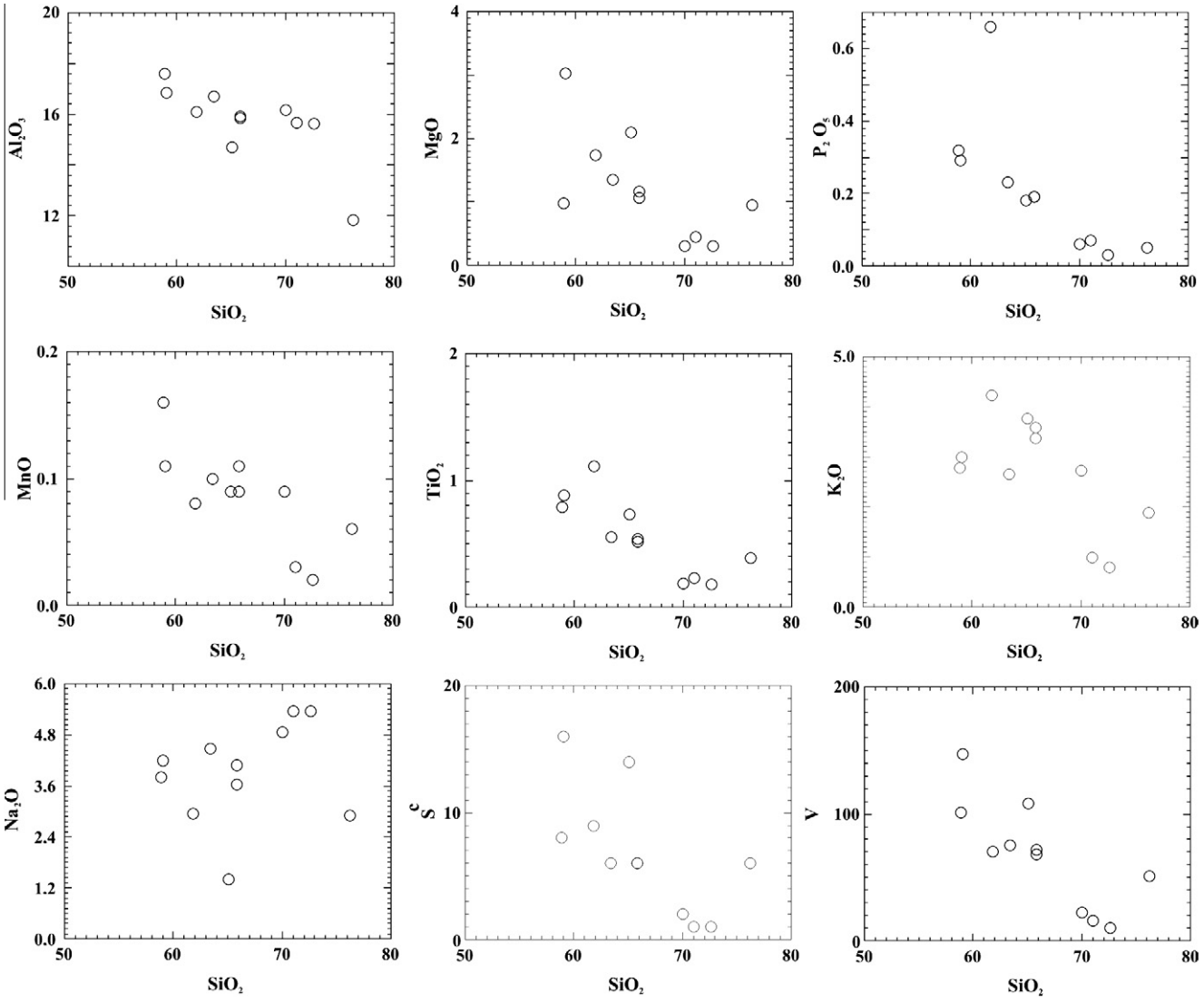

Fig. 5. Selected Harker diagrams from the Mylonitic granitoids from Santa Marta.

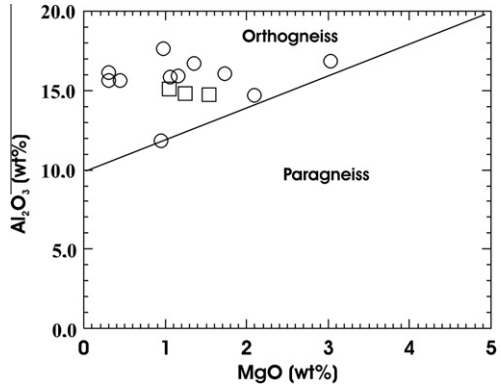

Fig. 6. Protolith discrimination diagram (Marc, 1992). Circles = Santa Marta Mylonites, squares = Cicuco High cores.

In the ACNK vs. ANK diagram all of the rocks are clearly subalkaline, and they plot between the metaluminous and peraluminous fields (Fig. 8). The aluminium saturation index (ASI) is below 1.1 for the mylonitic granitoids, within the range of the I-type granitoids (Chappell and White, 1992). The peraluminous nature of two of the samples was probably related to the presence of Biotite in the protoliths, together with the formation of additional micaceous minerals during deformation. In contrast the Cicuco High granitoid samples show ASI values >1.2, which correlates the with the S-type granitoids suggested by Chappell and White (1992).

Chondrite normalized patterns for rare earth elements (REE) are strongly fractionated with enriched light rare earth elements (LREE) ($(La/Sm)_N$ = 2.33–5.31 and 2.86–2.99) and $(La/Yb)_N$ = 4.7–29.9 and 5.9–7.9 for the SM and LMB respectively (Fig. 9A). Most of the granitoids show a well defined negative Eu anomaly, with Eu/Eu^* between 0.53–0.96 and 0.41–0.60 attesting for significant plagioclase fractionation. Three of the more silica rich rocks from the mylinotitic belt of Santa Marta have the lowest REE contents and are characterized by a weak to strong Eu/Eu^* positive anomaly, that is possibly related to a cumulate origin (Cullers and Graff, 1984).

Trace elements from both granitoid series are characterized by a relative enrichment in the alkali elements (K, Rb, Ba) and Th, with a weak depletion in high field strength elements (Hf, Sm, Y, Yb)

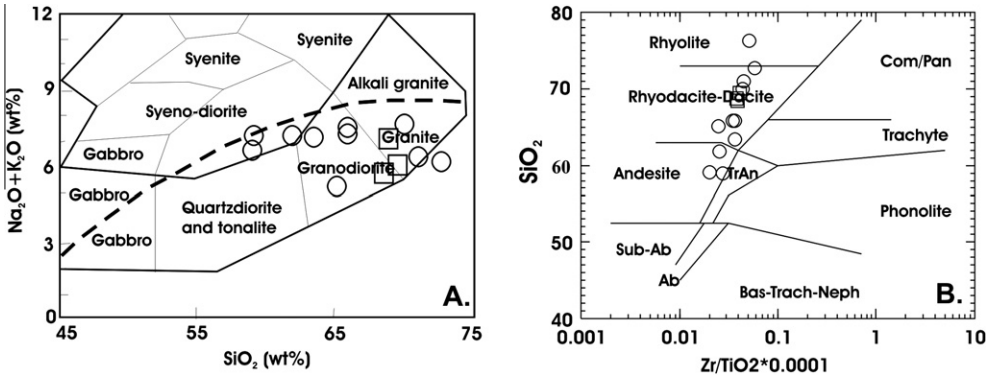

Fig. 7. (A) TAS modified classification diagram of plutonic igneous rocks (Wilson, 1989). (B) SiO_2-(Zr/TiO_2) after Winchester and Floyd (1977). Circles = Santa Marta Mylonites, squares = Cicuco High cores.

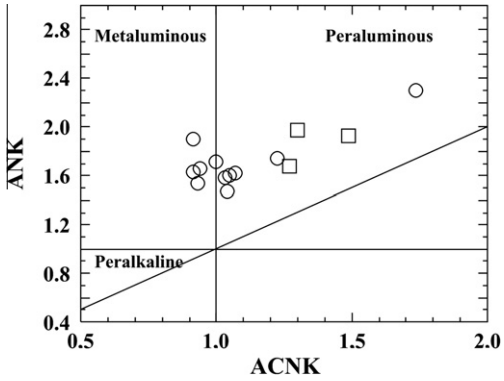

Fig. 8. ACNK vs. ANK discrimination diagram. Circles = Santa Marta Mylonites, squares = Cicuco High cores.

when normalized against the primitive mantle (Fig. 9B). The geochemical compositions of granitoid rocks usually provide insights about tectonic settings (Pearce et al., 1984; Harris et al., 1986; Pearce, 1996). Within the Rb–Nb–Y and Ta–Yb diagrams of Pearce et al. (1984) all the data points plot within the volcanic arc field (VAG) (Fig. 10). Similarly, mantle normalized trace element patterns show negative Nb, Ta and TiO_2 (Fig. 9B) anomalies that support their formation as subduction-related magmas.

4.4. Mineral chemistry

Due to their importance for regional understanding of a scarcely exposed basement domains, we have analyzed the mineral chemistry of Biotite porphyroclasts from the granitoid recovered at the Cicuco-2A well in the lower Magdalena Valley. The chemical

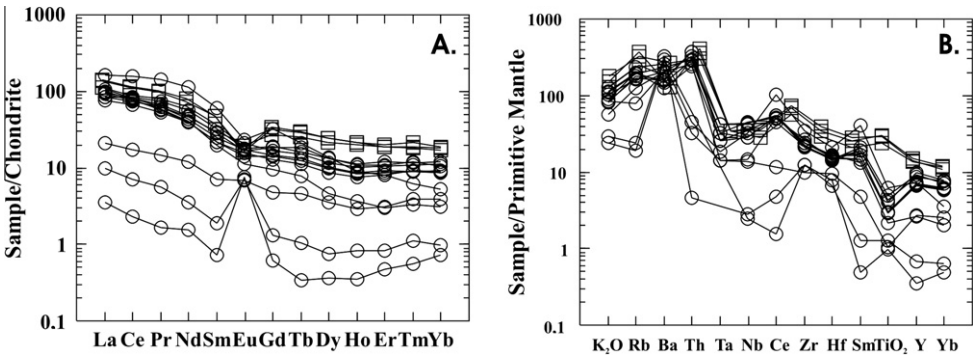

Fig. 9. (A) Rare earth element diagrams. (B) Normalized multielemental diagram. Circles = Santa Marta Mylonites, squares = Cicuco High cores.

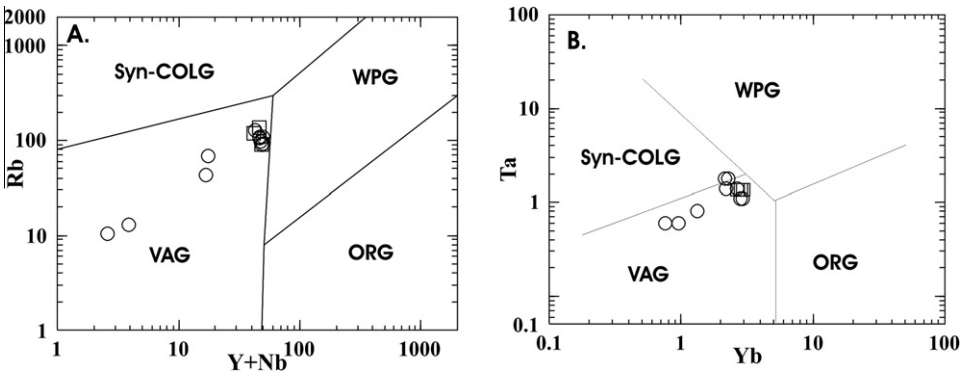

Fig. 10. Granitoid tectonic discrimination diagram (Pearce et al., 1984). Circles = Santa Marta Mylonites, squares = Cicuco High cores.

Table 3
Mineral chemistry from the Cicuco-2A sample (lower Magdalena Valley).

Sample	1	2	3	4
SiO_2	35.142	32.477	34.040	34.194
TiO_2	1.753	1.657	1.542	1.901
Al_2O_3	18.681	20.852	19.726	19.409
FeO	22.654	23.219	22.014	21.969
MnO	0.192	0.178	0.184	0.197
MgO	7.621	7.590	7.070	7.081
CaO	0.004	0.126	0.090	0.034
Na_2O	0.026	0.050	0.057	0.091
K_2O	8.928	7.034	8.843	8.893
Si	5.398	5.108	5.326	5.336
Al iv	2.602	2.892	2.674	2.664
Al vi	0.781	0.974	0.964	0.906
Al total	3.382	3.866	3.638	3.570
Ti	0.203	0.196	0.181	0.223
Fe	2.910	3.054	2.881	2.867
Mn	0.025	0.024	0.024	0.026
Mg	1.745	1.780	1.649	1.647
Ca	0.001	0.021	0.015	0.006
Na	0.008	0.015	0.017	0.028
K	1.749	1.411	1.765	1.770
Total	19.751	19.476	19.633	19.637
Fe/Fe + Mg	0.625	0.632	0.636	0.635

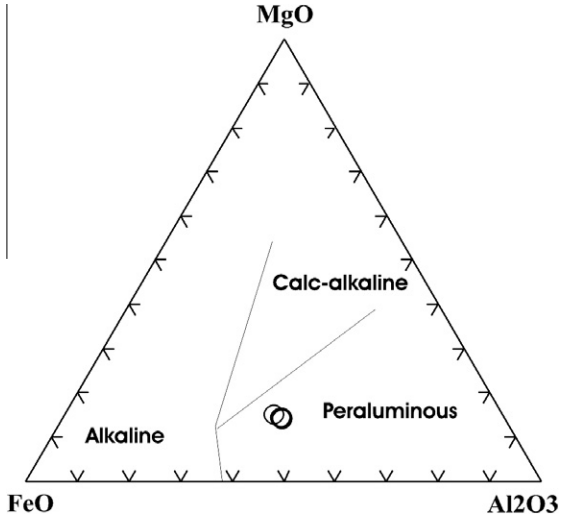

Fig. 11. Biotite composition magmatic discrimination diagram (Abdel-Rahman, 1994). Analyzed Biotites are from the Cicuco-2 High.

composition of Biotites are used as an additional discriminator of magma characteristics (Abdel-Rahman, 1994; Batchelor, 2003). Analytical results are shown in Table 3.

Biotites have homogenous Fe/Fe + Mg and Al iv values between 0.625–0.636 and 2.62–2.89. When plotted in the FeO–MgO–Al_2O_3 discrimination diagram (Abdel-Rahman, 1994), results confirm the peraluminous nature of the Cicuco High grantoids (Fig. 11).

5. Discussion and tectonic implications

Field and geochemical data have shown that the mylonitic granitoids from the northeastern segment of the Santa Marta Massif were formed within a convergent arc related setting. This arc grew during the Permian between 288 Ma and 264 Ma as seen by the U/Pb zircon crystallization ages, and intrudes a Paleozoic metamorphic basement that has experienced previous amphibolite facies metamorphism (Cardona-Molina et al., 2006) Inherited Grenvillian zircons are similar to the ages from the basement rocks found adjacent to this arc within the SM, and also constitute the backbone of the Eastern Colombian Andes (Cordani et al., 2005), and may suggest that this arc was probably built close to the northern South American margin. Relict oriented myrmekites and kinked plagioclase surrounded by the micaceous fabric suggest a high temperature deformational event with temperatures $\geqslant$450 °C (Passchier and Trouw, 1996). Remnants of Permian magmatism have been also found along different segments of the northern Andes (Fig. 12), including the Sierra de Perijá, Maracaibo Lake, and the El Baul massif in Venezuela (Espejo et al., 1980; Dasch, 1982; Feo-Codoecido et al., 1984; Viscarret et al., 2007) as well as in the island of Trinidad (Speed et al., 1997). Farther south in the Central Cordillera of the Colombian Andes, Early Permian xenocrysts have been reported in S-type Triassic granitoids and paragneisses (Ordoñez and Pimentel, 2002; Vinasco et al., 2006; Ibañez-Mejía et al., 2008). Therefore, it is possible that they are part of the active Permian proto-Andean margin. Following the growth of this arc, there are evidences for a major switch in the regional tectonomagmatic evolution. The ca. 240 Ma S-type granitoids from the Cicuco High (Montes et al., 2010), and similar ca. 245 Ma Muscovite orthogneises from farther south in the Guajira region (Weber et al., 2010) have compositional characteristics that differ from the previous I-type arc granitoid, particularly their typical S-type signature. Íts also suggested that the continental arc affinity of this plutonism in the Cicuco High granitoids may reflect their origin due to the melting of the older Permian arc.

We suggest that the high temperature deformational event in the mylonites and the ca. 250 Ma Pb loss found in one of the samples from Santa Marta, together with the similar amphibole K–Ar age obtained by MacDonald and Hurley (1969) in a gneissic clast found in proximity to the studied mylonites are related to this event. Also some of the more aluminous and silica high sample from the Santa Marta Mylonites are potential vestiges of this event that must be considered in detail during future geochronological

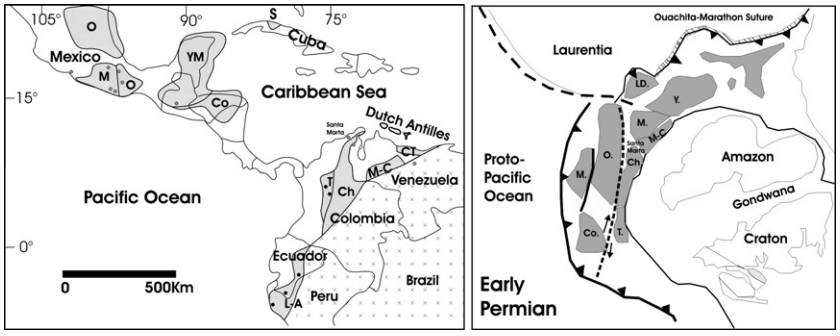

Fig. 12. Actual geography and Permian paleogeography of western Pangea including Colombian and Mexican terranes (modified from Weber et al. (2007) and reference therein).

research. The Permo-Triassic detrital zircon population found in the Late Cretaceous metasediments of Santa Marta and Guajira confirms the importance of this event in the region (Cardona et al., 2010; Weber et al., 2010). A major Early Triassic event has been also recognized in other segments the Northern Andes of Colombian and Ecuadorian (reviews in Noble et al. (1997), Ordoñez and Pimentel (2002), Vinasco et al. (2006), Weber et al. (2007)). Paleogeographic reconstructions have suggested the existence of a spatial geological overlapping between the Northern Andes and some of the Mexican and Central American Pre-Jurassic terranes during Late Paleozoic to Triassic agglutination of Pangea supercontinent (Pindell and Dewey, 1982; Pindell, 1985; Rowley and Pindell, 1989; Ruiz et al., 1999; Stewart et al., 1999; Dickinson and Lawton, 2001). In Middle America there is evidence of a similar switch from I-type to S-type magmatism with associated high temperature metamorphism (Weber et al., 2007; 2009; Estrada-Carmona et al., 2008). Within this context, different models have been proposed for the change from the Permiam to the Early Triassic tectonic events along both the northern Andes and Mexico: (1) an Alleghanian collision of several terranes trapped between the Laurentia–Gondwana collison, (2) the subduction of a thickened oceanic plate, (3) terrane accretion, or (4) strong plate coupling during the final stages of Pangea agglutination (Vinasco et al., 2006; Cawood and Buchan, 2007; Weber et al., 2007, 2009).

Due to the regional distribution of the Triassic event, we consider the subduction of a thickened crust the less feasible model. The Early Permian arc ages from Santa Marta and the continuity of magmatic activity until the Triassic post-dates the main Ouachita-Marathon and Alleghanian sutures linked to Laurentia–Gondwana interactions, where the tectonic activity may have ended by ca. 281 Ma (reviews in Ross (1986), Dickinson and Lawton (2001), Hatcher (2002), Torsvik and Cocks (2004), Nance and Linnemann (2008)). We therefore suggest that terrane accretion or strong plate coupling are the more appropriate mechanism to explain the Permian to Triassic tectonics. Within these models, the older Permian arc is related to the subduction of the Pacific plate at the western margin of Pangea, and can be also considered as part of a broader magmatic provinces that extend to other allochthonous Mexican terranes (Fig. 12, Yáñez et al., 1991, Ruiz et al., 1999; Torres et al., 1999; Dickinson and Lawton, 2001; Elías-Herrera and Ortega-Gutiérrez, 2002, Solari et al., 2001; Ducea et al., 2004; Weber et al., 2007).

Finally, the existence of an overimposed greenschist facies mylonitic event, together with the Ar–Ar Maastrichian ages found in low strain domains in the host rocks of the Los Muchachitos Gneiss (Cardona-Molina et al., 2006), is linked to the Late Cretaceous-Paleogene accretion of the Caribbean front.

Acknowledgements

ECOPETROL-ICP, INGEOMINAS and INVEMAR and the Project "Evolución Geohistórica de la Sierra Nevada de Santa Marta" are acknowledged for their support. Field discussions with F. Colmenares, G. Guzmán, and the GEOSEARCH LTDA Sierra Nevada team are fully appreciated. V. Arboleda is acknowledged for help during sampling of the granitoid cores. Discussions with C. Vinasco and M. Ibañez are highly appreciated. J. Duque, M. E. Velazquez and C. A. Salazar are acknowledged for helping with sample preparation. Key suggestions of two anonymous reviewers are highly appreciated. Analytical work was partially supported by a research grant from the Fundación para el Apoyo de la Investigación y la Cultura del Banco de la República de Colombia, Project 2289. A. Garcia-Casco is kindly acknowledged for access to microprobe analyses. Funding for the Arizona LaserChron Center is provided by NSF EAR-0443387. This is a contribution to Project 546 of the International Geological Correlation Program, "Subduction zones of the Caribbean".

References

Abdel-Rahman, A.-F.M., 1994. Nature of biotites from alkaline, calc-alkaline and peraluminous magmas. Journal of Petrology 35, 525–541.

Barbarin, B., 1999. A review of the relationships between granitoid types, Their origin and their geodynamic environments. LITHOS 46, 605–626.

Batchelor, R.A., 2003. Geochemistry of biotite in metabentonites and an age discrimnant, indicator of regional magma sources and potential correlating tool. Mineralogical Magazine 67, 807–817.

Bustamante, C., Cardona, A., Saldarriaga, M., García-Casco, A., Valencia, V., Weber, M., 2009. Metamorfismo de los esquistos verdes y anfibolitas pertenecientes a los Esquistos de Santa Marta, Sierra Nevada de Santa Marta (Colombia): ¿registro de la colisión entre el Arco Caribe y la margen Suramericana? Boletín de Ciencias de la Tierra, Universidad Nacional de Colombia.

Cardona, A., Cordani, U., Nutman, A., 2008a. U–Pb SHRIMP zircon, 40Ar/ 39Ar geochronology and Nd isotopes from gneissic and granitoid rocks of the Illescas massif, Perú: a southern extension of a fragmented Late Paleozoic orogen? In: VI South American Symposium on Isotope Geology San Carlos de Bariloche – Argentina (Extended Abstracts).

Cardona, A., Duque, J., Ruiz, J., Valencia, V., Bayona, G., Jaramillo, C., Ojeda, G., Orozco, M.T., 2008b. Geochronology and tectonic implications of granitoids rocks from the northwestern Sierra Nevada de Santa Marta and sourronding basins, northeastern Colombia: Late Cretaceous to Paleogene convergence, accretion and subduction interactions between the Caribbean and South American plates. 18va Conferencia Geológica del Caribe. República Dominicana, 24–29 de Marzo.

Cardona-Molina, A., Cordani, U.G., MacDonald, W., 2006. Tectonic correlations of pre-mesozoic crust from the northern termination of the Colombian Andes, Caribbean region. Journal of South American Earth Sciences 21, 337–354.

Cawood, P.A., Buchan, C., 2007. Linking accretionary orogenesis with supercontinent assembly. Earth-Science Reviews 82, 217–256.

Cerón, J.F., Kellogg, J.N., Ojeda, G.Y., 2007. Basement configuration of the northwestern South America–Caribbean margin from recent geophysical data. Ciencia, Tecnología y Futuro 3, 25–49.

Chappell, B.W., White, A.J.R., 1992. And S-type granites in the Lachlan Fold Belt. Transaction of the Royal Society of Edinburgh: Earth Sciences 83, 1–26.

Chew, D.M., Magna, T., Kirkland, C.L., Miškovic, A., Cardona, A., Spikings, A., Schaltegger, U., 2008. Detrital zircon fingerprint of the Proto-Andes: evidence for a neoproterozoic active margin? Precambrian Research 167, 186–200.

Colletta, B., Roure, F., de Toni, B., Loureiro, D., Passalacqua, H., Gou, Y., 1997. Tectonic inheritance, crustal architecture, and contrasting structural styles in the Venezuela Andes. Tectonics 5, 777–794.

Cordani, U.G., Cardona, A., Jimenez, D., Liu, D., Nutman, A.P., 2005. Geochronology of Proterozoic basement inliers from the Colombian Andes: tectonic history of remnants from a fragmented Grenville belt. In: Vaughan, A.P.M., Leat P.T., Pankhurst, R.J. (Eds.), Terrane Processes at the Margins of Gondwana. Geological Society of London, Special Publication, vol. 246. pp. 329–346.

Cullers, R.L., Graf, J.L., 1984. Rare earth elements in igneous rocks of the continental crust; intermediate and silicic rocks; ore petrogenesis. In: Henderson, P. (Ed.), Rare earth Element Geochemistry. Developments in Geochemistry. Elsevier, pp. 275–316.

Dasch, L.E., 1982. U–Pb Geochronology of the Sierra de Perijá. Ph.D. Thesis. Case Western Reserve University, 163 p.

Dickinson, W.R., Lawton, T.F., 2001. Carboniferous to Cretaceous assembly and fragmentation of México. Geological Society of America Bulletin 113, 1142–1160.

Ducea, M.N., Gehrels, G.E., Shoemaker, S., Ruiz, J., Valencia, V.A., 2004. Geologic evolution of the Xolapa complex, southern México: evidence from U–Pb zircon geochronology. Geological Society of America Bulletin 116, 1016–1025.

Duque-Caro, H., 1979, Major structural elements and evolution of northwestern Colombia. In: Watkins, J.S., Montadert, L., Dickerson, P.W. (Eds.), Geological and Geophysical Investigations of Continental Margins. AAPG Memoir, vol. 29. pp. 329–351.

Elías-Herrera, M., Ortega-Gutiérrez, F., 2002. Caltepec fault zone: an early Permian dextral transpressional boundary between the Proterozoic Oaxacan and Paleozoic Acatlán complexes, southern México, and regional tectonic implications. Tectonics 21, 1–19.

Espejo, A., Etchart, H., Cordani, U., Kawashita, K., 1980. Geocronología de intrusívas ácidas en la Sierra de Perijá, Venezuela. Boletín Dirección, General de Minas y Geología XIV, 245–254.

Estrada-Carmona, J., Weber, B., Hecht, L., Martens, U., 2008. P-T-t trajectory of metamorphic rocks from the central Chiapas Massif Complex: the Custepec unit, Chiapas, Mexico. Revista Mexicana de Ciencias de la Tierra 26, 243–259.

Feo-Codoecido, G., Smith, F., Aboud, N., Di Giacomo, E., 1984. Basement Paleozoic rocks of the Venezuelan Llanos basin. Geological Society of America, Memoir 162, 175–187.

Gehrels, G., Valencia, V., Ruiz, J., 2008. Enhanced precision, accuracy, efficiency, and spatial resolution of U–Pb ages by laser ablation-multicollector-inductively coupled plasma-mass spectrometry. Geochemistry Geophisics Geosystems. doi:10.1029/2007GC001805.

Harris, N.B.W., Pearce, J.A., Tindle, A.G., 1986. Geochemical characteristics of collision-zone magmatism. In: Coward, M.P., Ries, A.C. (Eds.), Collision Tectonics. Geological Society Special Publication, vol. 19. pp. 67–81.
Hatcher, R.D., 2002. Alleghanian (Appalachian) orogeny, a product of zipper tectonics: rotational transpressive continent–continent collision and closing of ancient oceans along irregular margins. In: Martínez Catalán, Hatcher, R.D., Arenas, R., Díaz-García, F. (Eds.), Variscan-Appalachian Dynamics: The building of the late Paleozoic Basement. Boulder, Colorado, Geological Society of America Special Paper, vol. 364. pp. 199–208.
Hollings, P., Wyman, D., 2005. The geochemistry of trace elements in igneous systems: principles and examples from basaltic systems. In: Linnen, R.L., Samson, I.M. (Eds.), Rare-element Geochemistry and Mineral Deposits: Geological Association of Canada, GAC Short Course Notes, vol. 17. pp. 1–16.
Ibañez-Mejía, M., Jaramillo-Mejía, J.M., Valencia, V., 2008. U–Th/Pb zircon geochronology by multicollector LA-ICP-MS of the Samaná Gneiss: a Middle Triassic syn-tectonic body in the Central Andes of Colombia, related to the latter stages of Pangea assembly. In: VI South American Symposium on Isotope Geology San Carlos de Bariloche – Argentina (Extended Abstracts).
Kellogg, J.N., 1984. Cenzoic tectonic history of the Sierra de Perijá, Venezuela-Colombia, and adjacent basins. Geological Society of America, Memoir 162, 239–261.
MacDonald, W.D., Hurley, P.M., 1969. Precambrian gneisses from northern Colombia, South America. Geological Society of America Bulletin 80, 1867–1872.
MacDonald, W., Doolan, B., Cordani, U., 1971. Cretaceous-early tertiary metamorphic age values from the South Caribbean. Geological Society of America Bulletin 82, 1381–1388.
Macellari, C., 1995. Cenozoic sedimentation and tectonics of the southwestern Caribbean pull-apart basin, Venezuela and Colombia. In: Tankard, A., Suarez, S., Welsink, H. (Eds.), Petroleum basins of South America, vol. 62. AAPG Memoir, pp. 757–780.
Marc, D., 1992. Granites and rhyolites from the northwestern USA: temporal variation in magmatic processes and relations to tectonic setting. Transactions of the Royal Society of Edinburgh, Earth Sciences 83, 51–64.
Michard, A., 1989. Rare earth element systematics in hydrothermal fluids. Geochimica et Cosmochimica Acta 53, 745–750.
Montes, C., Guzmán, G., Bayona, G., Cardona, A., Valencia, V., 2010. Clockwise rotation of the Santa Marta Massif and Simultaneous Paleogene to Neogene deformation of the Plato-San Jorge and Cesar-Ranchería basins. Journal of South American Earth Sciences 29, 832–848.
Montes, C., Hatcher, R.D., Restrepo-Pace, P., 2005. Tectonic reconstruction of the northern Andean block: Oblique convergence and rotations derived from the kinematic of the Piedras-Girardot area, Colombia. Tectonophysics 399, 221–250.
Nance, R.D., Linnemann, U., 2008. The Rheic ocean: origin, evolution, and significance. GSA Today 18, 4–12.
Noble, S.R., Aspden, J.A., Jemelita, R., 1997. Northern Andean crustal evolution: New U–Pb geochronological constraints from Ecuador. Geological Society of America Bulletin 109, 789–798.
Ordoñez, O., Pimentel, M., 2002. Rb–Sr and Sm–Nd isotopic study of the Puqui complex, Colombian Andes. Journal of South American Earth Sciences 15 (2), 173–182.
Passchier, C.W., Trouw, R.A., 1996. Microtectonics. Springer. 288 p.
Pearce, J.A., 1996. Sources and settings of granitic rocks. Episodes 19, 120–125.
Pearce, J.A., Harris, N.B.W., Tindle, A.G., 1984. Trace element discrimination diagrams for the tectonic interpretation of granitic rocks. Journal of Petrology 25, 956–983.
Pindell, J., 1985. Alleghenian reconstruction and subsequent evolution of the gulf of México, Bahamas, and Proto Caribbean. Tectonics 4, 1–39.
Pindell, J., Dewey, J., 1982. Permo-Triassic reconstruction of western Pangea and the evolution of the gulf of Mexico/Caribbean region. Tectonics 1, 179–211.
Poole, F.G., Perry, W.J.Jr., Madrid, R.J., Amaya-Martínez, R., 2005. Tectonic Synthesis of the Ouachita-Marathon-Sonora orogenic Margin of Southern Laurentia: Stratigraphic and Structural Implications for Timing of Deformational Events and Plate-tectonic Model. Geological Society of America Special Paper, vol. 393. pp. 543–596.
Rabe, 1977. Zur Stratigraphie des ostandinen Raumes von Kolumbien. Giessner Geologishe Schriften. 223 p (With English Abstract).
Restrepo, J.J., Toussaint, J.F., Gonzalez, H., Cordani, U., Kawashita, K., Linares, E., Patricia, C., 1991. Precisiones geocronológicas sobre el occidente Colombiano. In: Simposio sobre magmatismo andino y su marco tectónico, Manizales, vol. 1. pp. 1–21.
Restrepo-Pace, A., Ruiz, J., Gehrels, G., Cosca, M., 1997. Geochronology and Nd isotopic data of Grenville-age rocks in the Colombian Andes: new constraints for Late Proterozoic-early Paleozoic paleocontinental reconstructions of the Americas. Earth and Planetary Science Letters 150 (3–4), 427–441.
Rollinson, H., 1993. Using Geochemical Data: Evaluation, Presentation, Interpretation. Longman, UK. 352 p.
Ross, C.A., 1986. Paleozoic evolution of southern margin of Permian basin. Geological Society of America Bulletin 97, 536–554.
Rowley, D.B., Pindell, J.L., 1989. End Paleozoic-early Mesozoic western Pangean reconstruction and its implications for the distribution of Precambrian and Paleozoic rocks around Meso-Cenozoic. Precambrian Research 42, 411–444.
Rubatto, D., 2002. Zircon trace element geochemistry: distribution coefficients and the link between U–Pb ages and metamorphism. Chemical Geology 184, 123–138.
Ruiz, J., Tosdal, R.M., Restrepo, P.A, Murillo-Muñeton, G., 1999. Pb isotope evidence for Colombian-southern Mexico connections in the Proterozoic, In: Ramos, V.A., Keppie, J.D. (Eds.), Laurentia and Gondwana Connections before Pangea. GSA Special Paper, vol. 336. pp. P183–P198.
Solari, L.A., Dostal, J., Ortega-Gutiérrez, F., Keppie, J.D., 2001. The 275 Ma arc-related La Carbonara stock in the northern Oaxacan Complex of southern México: U–Pb geochronology and geochemistry. Revista Mexicana Ciéncias Geológica 18, 149–161.
Speed, R.C., Sharp, W.D., Folands, K.A., 1997. Late Paleozoic Granitoid Gneisses of northeastern Venezuela and the North America-Gondwana collision zones. Journal of Geology 105, 457–470.
Stacey, J.S., Kramers, J.D., 1975. Approximation of the terrestrial lead isotope evolution by a two-stage model. Earth and Planetary Science Letters 26, 207–221.
Stewart, J.H., Blodgett, R.B., Boucout, A.J., Carter, J.L., López, R., 1999. Exotic Paleozoic strata of Gondwana provenance near Ciudad Victoria, Tamaulipas, Mexico. In: Ramos, V.A., Keppie, J.D. (Eds.), Laurentia–Gondwana connections before Pangea. Geological Society of America Special Paper, vol. 336. pp. 227–252.
Taboada, A., Rivero, L., Fuenzalida, A., Cisternas, A., Philip, H., Bijwaard, Olaya, J., Rivera, C., 2000. Geodynamics of the northern Andes: subduction and intracontinental deformation (Colombia). Tectonics 19, 787–813.
Torres, R., Ruiz, J., Patchett, P.J., Grajales J.M., 1999. Permo-Triassic continental arc in eastern México: tectonic implications for reconstructions of southern North America. In: Bartolini, C.W., Wilson, J.L., Lawton, T.F. (Eds.), Mesozoic Sedimentary and Tectonic History of North-Central Mexico. Geological Society of America Special Paper, vol. 340. pp. 191–196.
Torsvik, T.H., Cocks, R.M., 2004. Earth geography from 400–250 Ma: a paleomagnetic, faunal and facies review. Journal of the Geological Society, London 161, 555–572.
Toussaint, J.F., 1993. Evolución geológica de Colombia, Precámbrico–Paleozóico, Universidad Nacional de Colombia, Medellín, 129 p.
Tschanz, C.M., Jimeno, A., Cruz, J., 1969. Geology of the Santa Marta area (Colombia). Instituto Nacional de Investigaciones Geológico Mineras, Informe, vol. 1829. 288 p.
Tschanz, C.M., Marvin, R.F., Cruz, J., 1974. Geologic evolution of the Sierra Nevada de Santa Marta area, Colombia. Geological Society of America Bulletin 85, 273–284.
Valencia, V.A., Ruiz, J., Barra, F., Gehrels, G., Ducea, M., Titley, S.M., Ochoa-Landin, L., 2005. U–Pb single zircon and Re-Os geochronology from La Caridad Porphyry Copper deposit: insights for the duration of magmatism and mineralization in the Nacozari District, Sonora, Mexico. Mineralium Deposita 40, 175–191.
Vinasco, C.J., Cordani, U., González, G., Weber, M., Pelaez, C., 2006. Geochronological, isotopic, and geochemical data from Permo-Triassic granitic gneisses and granitoids of the Colombian Central Andes. Journal of South American Earth Sciences 21, 355–371.
Viscarret, P., Wright, J., Urbani, F., 2007. Dataciones U/Pb SHRIMP en circón de rocas del Macizo El Baúl, Cojedes, Venezuela. In: IX Congreso Venezolano, Caracas, 22–25 de octubre, CD con resúmenes.
Weber, M., Cardona, A., Valencia, V., García-Casco, A., Tobon, M., Zapata, S., 2010. U/Pb detrital zircon provenance from Late Cretaceous metamorphic units of the Guajira Peninsula, Colombia: tectonic implications on the collision between the Caribbean arc and the South American margin. Journal of South American Earth Sciences 29, 805–816.
Weber, B., Irondo, A., Premo, W.R., Hecht, L., Schaaf, P., 2007. New insights into the history and origin of the southern Maya block, SE México: U–Pb–SHRIMP zircon geochronology from metamorphic rocks of the Chiapas massif. International Journal of Earth Sciences 96, 253–269.
Weber, B., Valencia, V.A., Schaaf, P., Ortega-Gutierrez, F., 2009. Detrital zircon ages from the Lower Santa Rosa Formation. Chiapas: Implications on Regional Paleozoic Stratigraphy 26, 260–276.
Wilson, M., 1989. Igneous Petrogenesis, Seventh reprinted. Chapman & Hall. 467 p.
Winchester, J.A., Floyd, P.A., 1977. Geochemical discrimination of different magma series and their differentiation products using immobile element. Chemical Geology 20, 325–343.
Yáñez, P., Ruiz, J., Patchett, P.J., Ortega-Gutiérrez, F., Gehrels, G.E., 1991. Isotopic studies of the Acatlan complex, southern Mexico – implications for Paleozoic North American tectonics. Geological Society of America Bulletin 103, 817–828.
Zhou, X., Sun, T., Weizhou, S., Shu, L., Niu, L., 2006. Petrogenesis of Mesozoic granitoids and volcanic rocks in South China: a response to tectonic evolution. Episodes 29, 26–33.